ELSEVIER

Analysis of the spin-dipole transmission mechanism for NMR spin–spin coupling constants using orbital contributions, spin polarization, and spin-dipole energy density distribution

Jürgen Gräfenstein, Dieter Cremer *

Department of Theoretical Chemistry, Göteborg University, Reutersgatan 2, S-41320 Göteborg, Sweden

Abstract

For the analysis of the spin-dipole (SD) term of the indirect NMR spin–spin coupling constant, the SD spin-polarization distribution and the SD energy density distribution are derived and used to explain magnitude and sign of the SD term. Orbital pairs (occupied, virtual) are identified that are most important for the SD spin–spin coupling mechanism. The induction of strong SD spin-polarization requires low excitation energies and complementing nodal properties of zeroth and first-order orbitals. The SD components for $^1J(CC)$ of typical CC bonds are analyzed. The SD term is a sensitive antenna for detecting the π-character of a bond.
© 2004 Elsevier B.V. All rights reserved.

1. Introduction

Magnetic properties of molecules can be used as sensitive indicators for their electronic structure and their bonding features [1–3]. This was amply demonstrated in the case of aromatic or antiaromatic molecules. Energy or geometry criteria are often insufficient to quantify the degree of (anti)aromaticity of a given compound [4–6]. However, NMR chemical shifts, magnetic susceptibilities, susceptibility exaltations or susceptibility anisotropies provide sensitive measures for the degree of electron delocalization in a molecule [4]. Some of the magnetic properties such as the magnetic susceptibility exaltation are not directly measured but derived within a given model. Others are not accessible to experiment at all and have to be calculated. An example for such properties are the nuclear independent chemical shifts (NICS) [7,8], which provide a sensitive measure for the degree of chemical shielding at a representative point in a molecule so that a comparison of NICS values for different molecules leads to a better insight into electronic structure

features of molecules, which is not provided by energy or electron density properties.

Next to NMR chemical shieldings, indirect NMR spin–spin coupling constants (SSCCs) are highly sensitive antennas for special features of the electronic structure of a molecule [1–3]. They can provide information on the electron system along a chain of bonds connecting two coupling nuclei in a molecule. The one-bond SSCC $^1J(CC)$ should provide a direct measure of the CC bond provided one is able to decode the spin–spin coupling mechanism and relate it to features of the chemical bond. In the literature, there are numerous experimental investigations attempting to explain bond features with NMR SSCCs [1]. Best known are the attempts of NMR spectroscopists to relate the $^1J(C,C)$ and $^1J(C,H)$ coupling constants in hydrocarbons to the s-character of the corresponding bond localized molecular orbitals (LMOs), the CC bond length, the bond order, or the π-character of a CC bond [9–16]. These attempts turned out to lead to useful relationships and corroborated the idea that the SSCC is an important descriptor of the chemical bond.

The present work is the fourth and last step to decode the spin–spin coupling mechanism for the four Ramsey

---

* Corresponding author. Fax: +46-31-77-35-590.
E-mail address: cremer@theoc.gu.se (D. Cremer).

terms of the indirect SSCC [17]. In previous work, we developed the coupled perturbed density functional theory (CP-DFT) method to calculate the Fermi contact (FC), the paramagnetic spin–orbit (PSO), the diamagnetic spin–orbit (DSO), and the spin dipole (SD) term of the indirect SSCC [18] and to partition the total SSCC and its Ramsey terms into one- and two-orbital contributions [19,20]. Each FC orbital term can be described by the FC spin density distribution, which itself is a product of zeroth-order and first-order spin orbitals where orbitals as well as FC spin density distribution can be graphically represented [19,20]. The analysis of the first-order orbitals and the FC spin density distribution led to an explanation of the dihedral angle dependence of vicinal SSCCs, the influence of lone pair electrons on the spin–spin coupling mechanism, and the development of advanced Dirac vector models, which provide an easy understanding of the sign of the FC term in n-bond SSCCs $^nJ(A,B)$ [19,20]. The DSO and PSO terms as well as their orbital contributions can be explained with the help of the DSO and PSO current densities and the DSO and PSO density distributions [21]. In this way, the p_σ- and p_π-electron currents in CC multiple bonds could be described and sign and magnitude of the DSO and PSO terms of a series of SSCC $^1J(CC)$ with single and multiple bond character could be explained [21].

The **J-OC-PSP** (decomposition of J into Orbital Contributions using Orbital Currents and Partial Spin Polarization) method [19,20] comprising these features proved very useful to understand spin–spin coupling in conjugated hydrocarbons [22,23] and across the H-bonds of proteins [24,25]. In this Letter, we present the last corner stone of the analysis, namely the detailed analysis of the SD term. The understanding of the SD coupling mechanism turns out to be desirable because in previous work [21,22] we could show that the π-character of a CC bond is reflected by the magnitude of the non-contact terms $NC = PSO + SD + DSO \approx PSO + SD$ where the DSO is so small that it normally can be neglected. Since it is possible to assess the NC term of one-bond CC SSCCs from measured $^1J(C,C)$ and $^1J(C,H)$ values of a hydrocarbon, it is important to decode the relationship between PSO term, SD term, and CC bond strength.

The first task of this goal was fulfilled in previous work: [21] We analyzed the relationship between the π bond order and the PSO term for acetylene (**1**), ethylene (**2**), and ethane (**3**). The π bonds in **1** and **2** clearly manifest themselves in $^1J(CC)$. However, the sign and size of the effects depend on the details of the bond situation in a quite complicated way, and it is difficult to establish practically useful relationships between $^1PSO(CC)$ and the π-bond order. This became clear when analyzing the π-character of the formal single bonds in a number of conjugated or hypercon-

jugated hydrocarbons [22]. In the present Letter, we investigate whether the SD spin–spin coupling mechanism provides a more efficient basis for the assessment of the π-character of CC bonds. For this purpose, we calculate $^1J(CC)$ and the four Ramsey terms for **1**, **2** and **3** at the CP-DFT level of theory [18], decompose the SD term in orbital contributions [19], and analyze them in dependence of the π-character of the CC bond.

There are five basic questions that we want to answer in this work: (1) Which properties have to be defined to investigate the isotropic SD term, its Cartesian components, and its orbital contributions? (2) Can one derive general rules to understand sign and magnitude of the SD term? (3) How is the SD term of $^1J(CC)$ related to the electronic structure of the molecule, especially to the σ- or π-character of the CC bond? (4) Can one assess the π-character of a CC bond from the SD term of its SSCC $^1J(CC)$? (5) Is the SD term a suitable antenna for understanding the electronic structure of a molecule in general?

For the purpose of answering these questions, we develop in Section 2 a generally applicable procedure to analyze the SD term of the indirect SSCC. This implies the derivation of the SD spin polarization distribution and the SD energy density distribution, which are defined in analogy to the PSO current density distribution and PSO energy density distribution introduced in [21]. The calculated SD values of the SSCCs in **1**, **2**, and **3** are analyzed in terms of orbital contributions, SD spin polarization, and SD energy density in Section 3. Section 4 summarizes the conclusions of this work. Some technical aspects are discussed in Appendix A.

2. Theory

The microscopic theory of NMR spin–spin coupling was derived by Ramsey [17] who employed second-order perturbation theory with respect to the magnetic moments of the two coupling nuclei A and B. According to this theory, one considers that nucleus B (called perturbing nucleus in the following) perturbs by its magnetic moment the electron system, which in turn gives rise to a magnetic field at the position of the responding nucleus A. The reduced SSCC K_{AB} is represented as a sum of FC, SD, DSO, and PSO term (see Eqs. (1)–(4)) [17,18]:

$$K_{AB}^{FC} = \frac{2}{3} \sum_{k\sigma}^{occ} \langle \psi_{k\sigma}^{(0)} | \mathbf{h}_A^{FC} | \vec{\psi}_{k\sigma}^{(B),FC} \rangle, \tag{1}$$

$$K_{AB}^{SD} = \frac{2}{3} \sum_{k\sigma}^{occ} \langle \psi_{k\sigma}^{(0)} | \mathbf{h}_A^{SD} | \vec{\psi}_{k\sigma}^{(B),SD} \rangle, \tag{2}$$

$$K_{AB}^{\text{DSO}} = \frac{2}{3} \sum_{k}^{occ} \langle \phi_{k}^{(0)} | Tr\, \underline{\underline{h}}_{AB}^{\text{DSO}} | \phi_{k}^{(0)} \rangle, \tag{3}$$

$$K_{AB}^{\text{PSO}} = -\frac{4}{3} \sum_{k}^{occ} \langle \phi_{k}^{(0)} | \mathbf{h}_{A}^{\text{PSO}} | \vec{\phi}_{k}^{(B),\text{PSO}} \rangle, \tag{4}$$

where the FC, SD, DSO, and PSO operators are defined by Eqs. (5)–(8):

$$\mathbf{h}_{A}^{\text{FC}} = \left\{ \frac{4\pi\varepsilon_0\hbar^3}{e^3 m} \right\} \frac{8\pi}{3} \alpha^2 \delta(\mathbf{r}_A)\mathbf{s}, \tag{5}$$

$$\mathbf{h}_{A}^{\text{SD}} = \left\{ \frac{4\pi\varepsilon_0\hbar^3}{e^3 m} \right\} \alpha^2 \left[3\frac{(\mathbf{s} \cdot \mathbf{r}_A)\mathbf{r}_A}{r_A^5} - \frac{\mathbf{s}}{r_A^3} \right], \tag{6}$$

$$\underline{\underline{h}}_{AB}^{\text{DSO}} = \left\{ \frac{1}{m} \left(\frac{4\pi\varepsilon_0\hbar^2}{e^3} \right)^2 \right\} \alpha^4 \left(\frac{\mathbf{r}_A}{r_A^3} \cdot \frac{\mathbf{r}_B}{r_B^3} \underline{\underline{I}} - \frac{\mathbf{r}_A}{r_A^3} \circ \frac{\mathbf{r}_B}{r_B^3} \right), \tag{7}$$

$$\mathbf{h}_{A}^{\text{PSO}} = \left\{ \frac{4\pi\varepsilon_0\hbar^3}{e^3 m} \right\} \alpha^2 \frac{\mathbf{r}_A}{r_A^3} \times \nabla. \tag{8}$$

Symbol $\circ$ denotes a tensor product and $\delta(\mathbf{r}_A)$ is the Dirac operator at position $\mathbf{r}_A$. The position of nucleus N (A or B) is given by vector $\mathbf{R}_N$ the vector $\mathbf{r}_N = \mathbf{r} - \mathbf{R}_N$ defines position and distance of an electron relative to nucleus N, ε_0 is the dielectric constant of the vacuum, α is Sommerfeld's fine structure constant, $\underline{I}$ is the unit tensor, and $\mathbf{s}$ is the electron spin in units of $\hbar$. The prefactors enclosed in braces in Eqs. (5)–(8) become equal to one in atomic units. Operators $\mathbf{h}_{A}^{\text{FC}}$ $\mathbf{h}_{A}^{\text{SD}}$ represent 2×2 matrices with respect to the electron spin variables, i.e. the corresponding matrix elements are expressed in terms of spin orbitals ψ_{k}. The DSO and the PSO terms can be expressed in terms of space orbitals ϕ_{k}. Zeroth-order orbitals are denoted by superscript (0) and first-order orbitals resulting from the perturbing nucleus B by superscript (B). The indices of the occupied orbitals will be k,l,..., those of the virtual orbitals a,b,... The vectors $\vec{\psi}_{k}^{(B),X}$ and $\vec{\phi}_{k}^{(B),X}$ summarize the three first-order spin and space orbitals corresponding to the three components of $\mathbf{h}^{(B),X}$ ($X = \text{PSO,FC,SD}$).

The PSO and DSO terms describe the coupling between the two nuclei by orbital currents whereas the FC and SD terms account for the coupling mediated by spin polarization of the electron system. It has proven useful to split the nuclear magnetic field in two components: The field inside the (small but finite) nucleus gives rise to the FC term, which is the dominating term of the total SSCC in most cases. The effect of the extended dipole field outside the perturbing nucleus is covered by the SD term. The SD term is often negligible and sizable only in particular cases, which is just why this term is a prospective indicator for the π-character of a bond.

In its general definition, the SSCC is a tensor with respect to the orientations of the perturbing and responding nuclei (see e.g. [17]), and the scalar SSCC as

given by Eqs. (1)–(8) is 1/3 the trace of the corresponding SSCC tensor. The scalar SSCC corresponds to spin–spin coupling averaged over all orientations of the perturbing nucleus and corresponds to the result from NMR measurements in gas phase or solution. For the purpose of investigating the electronic mechanism of magnetic spin–spin coupling, it is necessary to consider the individual diagonal components of the SSCC tensor, which specify the SSCC for a given orientation of the perturbing nucleus. The FC term is isotropic, whereas the SD term is orientation-dependent. The diagonal components of the SD term along a given direction $\mathbf{n}$ required to calculate the isotropic SD term have the form

$$K_{AB,\mathbf{nn}}^{\text{SD}} = \sum_{k\sigma}^{occ} \langle \psi_{k\sigma}^{(0)} | \left(\mathbf{n}\underline{\underline{h}}_{A}^{(B),\text{SD}}\mathbf{n} \right) | \psi_{k\sigma,\mathbf{n}}^{(B),\text{SD}} \rangle. \tag{9}$$

For $\mathbf{n} = x, y,$ or z, the products of $\mathbf{s}$ with $\mathbf{n}$ occurring in Eq. (9) (see also Eq. (6)) can be evaluated explicitly, and Eq. (9) can be expressed in terms of the space orbitals ϕ_{k}:

$$K_{AB,ii}^{\text{SD}} = \sum_{j} K_{AB,(ij)}^{\text{SD}}, \tag{10a}$$

$$K_{AB,(ij)}^{\text{SD}} = 2 \sum_{k}^{occ} \langle \phi_{k}^{(0)} | (h_{A,(ij)}^{\text{SD}}) | \phi_{k,(ij)}^{(B),\text{SD}} \rangle. \tag{10b}$$

The symbol (ij) denotes one of the six sub-components (xx), (yy), (zz), (xy), (xz), (yz) of the diagonal terms of the SD tensor: The first index i ($= x, y, z$) specifies the direction of the spin moment of the perturbing nucleus whereas the second index j ($= x, y, z$) gives a component of the associated dipole field. The first-order orbital with respect to the perturbation $h_{B,(ij)}^{\text{SD}}$ is given by the following equation:

$$\begin{aligned} \phi_{k,(ij)}^{(B),\text{SD}} &= \sum_{a} \frac{\langle \phi_{a}^{(0)} | F_{B,(ij)}^{\text{SD}} | \phi_{k}^{(0)} \rangle}{\epsilon_{a} - \epsilon_{k}} | \phi_{a}^{(0)} \rangle \\ &= \sum_{a} c_{ak,(ij)} | \phi_{a}^{(0)} \rangle, \end{aligned} \tag{11}$$

where

$$F_{B,(ij)}^{\text{SD}} = h_{B,(ij)}^{\text{SD}} + \tilde{F}_{B,(ij)}^{\text{SD}} \tag{12a}$$

and

$$\tilde{F}_{B,(ij)}^{\text{SD}} = \sum_{k}^{occ} \int d^3 r \frac{\delta F^{\text{SD}}}{\delta\phi_{k}(\mathbf{r})} \phi_{k,(ij)}^{(B),\text{SD}}. \tag{12b}$$

Eq. (12) clarifies that $F_{B,(ij)}^{\text{SD}}$ depends in a similar way on the first-order orbital $\phi_{k,(ij)}^{(B),\text{SD}}$ as the Kohn–Sham operator $\mathbf{F}$ depends on the Kohn–Sham orbitals. The sub-component $K_{AB,(ij)}^{\text{SD}}$ can now be explicitly written as

$$K_{AB,(ij)}^{\text{SD}} = \sum_{k,a} \frac{\langle \phi_{k}^{(0)} | h_{A,(ij)}^{\text{SD}} | \phi_{a}^{(0)} \rangle \langle \phi_{a}^{(0)} | F_{B,(ij)}^{\text{SD}} | \phi_{k}^{(0)} \rangle}{\epsilon_{k} - \epsilon_{a}}, \tag{13}$$

$$h_{A,(ij)}^{SD} = \alpha^2 \left(3 \frac{x_{A,i} x_{A,j}}{r_A^5} - \frac{1}{r_A^3} \right). \tag{14}$$

For the calculation of the diagonal terms of the SD tensor, the quadrupole potentials represented by operators $h_{A,(ij)}^{SD}$ and $h_{B,(ij)}^{SD}$ have to adopt the same orientation (if they have different orientations, the sub-components of the off-diagonal elements of the SD tensor will be obtained).

The sign of the SD sub-components $K_{AB,(ij)}^{SD}$ can be predicted by considering that $F_{B,(ij)}^{SD}$ is dominated by the operator $h_{B,(ij)}^{SD}$ which has the same symmetry character as operator $h_{A,(ij)}^{SD}$. If the product $\phi_k^{(0)} \phi_a^{(0)}$ has the same symmetry character with respect to nuclei A and B, then the matrix elements $\langle \phi_k^{(0)} | h_{A,(ij)}^{SD} | \phi_a^0 \rangle$ and $\langle \phi_a^{(0)} | F_{B,(ij)}^{SD} | \phi_k^0 \rangle$ possess the same sign and, because of $\epsilon_k - \epsilon_a < 0$, the sub-component $K_{AB,(ij)}^{SD}$ becomes negative. Conversely, if the product $\phi_k^{(0)} \phi_a(0)$ has opposite signature at nuclei A and B, then sub-component $K_{AB,(ij)}^{SD}$ will be positive.

The isotropic SD term can thus be expressed in terms of the six sub-components $K_{AB,(ij)}^{SD}$ defined in Eq. (13) according to

$$K_{AB}^{SD} = \frac{1}{3} \sum_{ij} K_{AB,(ij)}^{SD}. \tag{15}$$

Introducing the SD spin polarization distribution $m_{B,(ij)}^{SD}(\mathbf{r})$ and the SD energy density distribution $\varrho_{AB,(ij)}^{SD}(\mathbf{r})$

$$m_{B,(ij)}^{SD}(\mathbf{r}) = 2 \sum_k^{occ} \phi_k^{(0)}(\mathbf{r}) \phi_{k,(ij)}^{(B),SD}(\mathbf{r})$$
$$= 2 \sum_{ka} c_{ak,(ij)} \phi_k^{(0)}(\mathbf{r}) \phi_a^{(0)}(\mathbf{r}) \tag{16a}$$

$$\varrho_{AB,(ij)}^{SD}(\mathbf{r}) = h_{A,(ij)}^{SD} m_{B,(ij)}^{SD}(\mathbf{r}) \tag{16b}$$

the sub-components $K_{AB,(ij)}^{SD}$ can be rewritten as

$$K_{AB,(ij)}^{SD} = \int d^3 r h_{A,(ij)}^{SD} m_{B,(ij)}^{SD}(\mathbf{r}), \tag{17a}$$

$$= \int d^3 r \varrho_{AB,(ij)}^{SD}(\mathbf{r}). \tag{17b}$$

Here $m_{B,(ij)}^{SD}(\mathbf{r})$ is the spin polarization in i direction that will result through the SD coupling mechanism if the perturbing nucleus at B is oriented in direction j. The spin polarization distribution $m_{B,(ij)}^{SD}(\mathbf{r})$ is a useful tool to study the SD coupling mechanism. By graphically representing and analyzing $m_{B,(ij)}^{SD}(\mathbf{r})$ one can rationalize the first step of the SD coupling mechanism, viz. the spin polarization of the electron system through the perturbing nucleus. For an effective SD coupling, however, it is necessary that the perturbation generates a dipole polarization around the responding nucleus. It is therefore valuable to study in addition the spin polarization distribution weighted with the quadrupole potential $h_{A,(ij)}^{SD}$. The resulting SD energy density distribution determines

the actual value of the sub-component $K_{AB,(ij)}^{SD}$. From $\varrho_{AB,(ij)}^{SD}(\mathbf{r})$, one can derive two more SD energy densities:

$$\varrho_{AB,ii}^{SD}(\mathbf{r}) = \sum_j \varrho_{AB,(ij)}^{SD}(\mathbf{r}), \tag{18a}$$

$$\varrho_{AB}^{SD}(\mathbf{r}) = \frac{1}{3} \sum_i \varrho_{AB,ii}^{SD}(\mathbf{r}), \tag{18b}$$

which give the SD energy density of component ii and the isotropic SD energy density distribution. Integration of $\varrho_{AB,ii}^{SD}(\mathbf{r})$ gives the ii component of the SD term, whereas integration of $\varrho_{AB}^{SD}(\mathbf{r})$ generates the total isotropic SD coupling constant.

Eqs. (1)–(18) refer to the reduced spin–spin coupling constant, which reflects only the electronic coupling mechanism between the nuclei. The experimentally observed coupling constant J_{AB} depends in addition on the gyromagnetic ratios γ_A, γ_B of the two coupling nuclei

$$J_{AB} = \frac{\gamma_A \gamma_B}{h} K_{AB}. \tag{19}$$

Analogous relationships hold for the four Ramsey terms and their components. The J_{AB} are isotope-dependent. In the following, J_{AB} values will be specified for ^{13}C–^{13}C SSCC.

We calculated the SSCCs for **1**, **2**, and **3** at the CPDFT level of theory, using the B3LYP exchange and correlation functional [26–28] and the (11s,7p,2d/6s,2p)/[7s,6p,2d/4s,2p] basis set designed for the calculation of magnetic properties [29]. Calculations were carried out at the experimental geometry of **1** [30], **2** [31], and **3** [32]. SD spin polarization distributions and SD energy density distributions were calculated and plotted for planes containing the CC bond. For **2**, this plane was perpendicular to the molecular plane, i.e., the π (C1C2) orbital is intersected by the drawing plane. For **3**, the drawing plane contains the CC bond and two of the CH bonds. In all cases, the drawing plane is the yz plane and the CC bond direction defines the z direction. The calculated SD spin polarization distribution and the SD energy density distribution are represented in form of contour line plots, where the contour levels are given by a geometric progression with the ratio of $100^{1/5}$ between two subsequent contours. Orbital contributions of the SD term and its components were determined with the **J-OC-PSP** algorithm [19,20], All calculations were done with the COLOGNE 2003 program package [33].

3. Results and discussion

In Table 1, calculated and measured SSCCs $^1J(CC)$ are compared for the three molecules investigated. Also listed are the calculated Ramsey terms of the SSCCs

Table 1
The NMR SSCC ^1J(CC) and its Ramsey terms for **1**, **2**, and **3**[a]

	DSO	PSO	FC	SD	^1J(CC) *Calc.*	^1J(CC) *Exp.*[b]
1	0.07	8.38	181.67	11.60	201.73	169.7
2	0.08	−10.28	76.87	3.94	70.62	67.5
3	0.13	0.01	32.77	1.09	34.00	34.5

[a] All values in Hz as calculated at the CP-DFT/B3LYP/(11s,7p,2d/6s,2p)[7s,6p,2d/4s,2p] level of theory using experimental geometries [30–32].
[b] Experimental values from K. Jaakko, P. Lantto, J. Vaara, J. Jokisaari, J. Am. Chem. Soc. 120 (1998) 3993.

Table 2
Isotropic SD term and SD sub-components (ij) of ^1J(CC) for acetylene (**1**), ethylene (**2**), and ethane (**3**)[a]

Mol.	Isotropic	(xx)	(yy)	(zz)	(xy)	(xz)	(yz)
1	11.60	9.42	9.42	5.43	8.05	−1.40	−1.40
2	3.94	2.74	11.28	4.08	−0.20	−3.01	0.07
3	1.08	0.50	0.50	2.03	−0.01	0.06	0.06

[a] All values in Hz as calculated at the CP-DFT/B3LYP/(11s,7p,2d/6s,2p)[7s,6p,2d/4s,2p] level of theory using experimental geometries [30–32]. The CC bonds are oriented along the z axis, the H atoms in C_2H_4 are in the xz plane.

which reveal that despite the dominance of the FC term, PSO term and SD term become increasingly important with the π-character of the CC bond. However, contrary to the PSO term, the SD term is always positive and increases steadily with the bond order. Table 2 lists the (ij) sub-components of the isotropic SD term for **1**, **2**, and **3**. All diagonal sub-components are also positive and, with the exception of the (yy) sub-component, their magnitude increases with the number of π bonds. This gives already a confirmation that the SD term is an indicator of the π-character of the CC bond. There is an exponential increase of the isotropic SD term in dependence of the CC bond order (Fig. 1). Analysis of the sub-components (Fig. 1 and Table 2) reveals that the (xx) sub-component is responsible for this increase. The (yy) sub-component is largest for **2** rather than **1**. However its effect is partially compensated by the (xy) sub-component (minimum for **2**) so that their sum behaves similarly as the (zz) sub-component, which in-

creases linearly with the bond order. Since the remaining terms are relatively small in magnitude (Table 2), the isotropic SD term is dominated by the (xx) sub-component, which in turn can be used to describe the π-bond character of a CC bond.

Although there seems to be confirmation that the SD term of ^1J(CC) can be used as an indicator for the CC bond strength, we have to concede that both sign and magnitude of the SD sub-components are not clear and therefore the relationship between SD term and bond order could be coincidental. It is necessary to analyze the various terms in Table 2 both with regard to their individual orbital contributions and in terms of the associated SD spin polarization and the SD energy density distribution. Such an analysis will disclose the relationship between electronic structure and SD term so that the role of the latter as a sensitive antenna for π-bonding can be established on physical rather than statistical grounds.

Figs. 2a–e represent contour line diagrams of the sub-components of the SD spin polarization distribution for molecule **1**. For the understanding of these diagrams one has to consider that (a) the perturbing nucleus is C2; (b) the SD spin polarization distribution in the immediate vicinity of the C2 nucleus is determined by its dipole vector field where α-spin is assumed for the perturbing nucleus; (c) the SD spin polarization beyond the immediate vicinity of C2 is determined by the nodal structure of the occupied and virtual orbitals dominating the value of $m_{B,(ij)}^{SD}$ which in turn depends on the coefficients $c_{ak,(ij)}$ of Eq. (11), i.e. the magnitude of the matrix elements $\langle \phi_a^{(0)}|F_{B,(ij)}^{SD}|\phi_k^{(0)}\rangle$ divided by the orbital energy differences $\epsilon_a - \epsilon_k$; (d) all six (ij) sub-components of the SD spin polarization distribution have to be considered to derive the total SD spin polarization distribution; and (e) the corresponding SD energy density distribution is obtained by multiplication with the quadrupole potential of the responding nucleus.
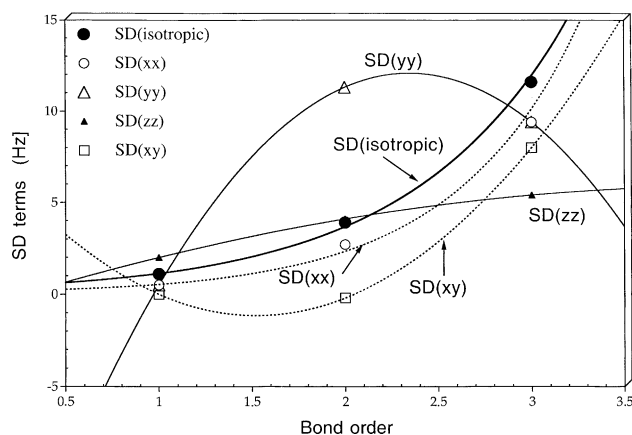

Fig. 1. Representation of the isotropic SD term and its sub-components as a function of the CC-bond order of acetylene (**1**), ethylene (**2**), and ethane (**3**).
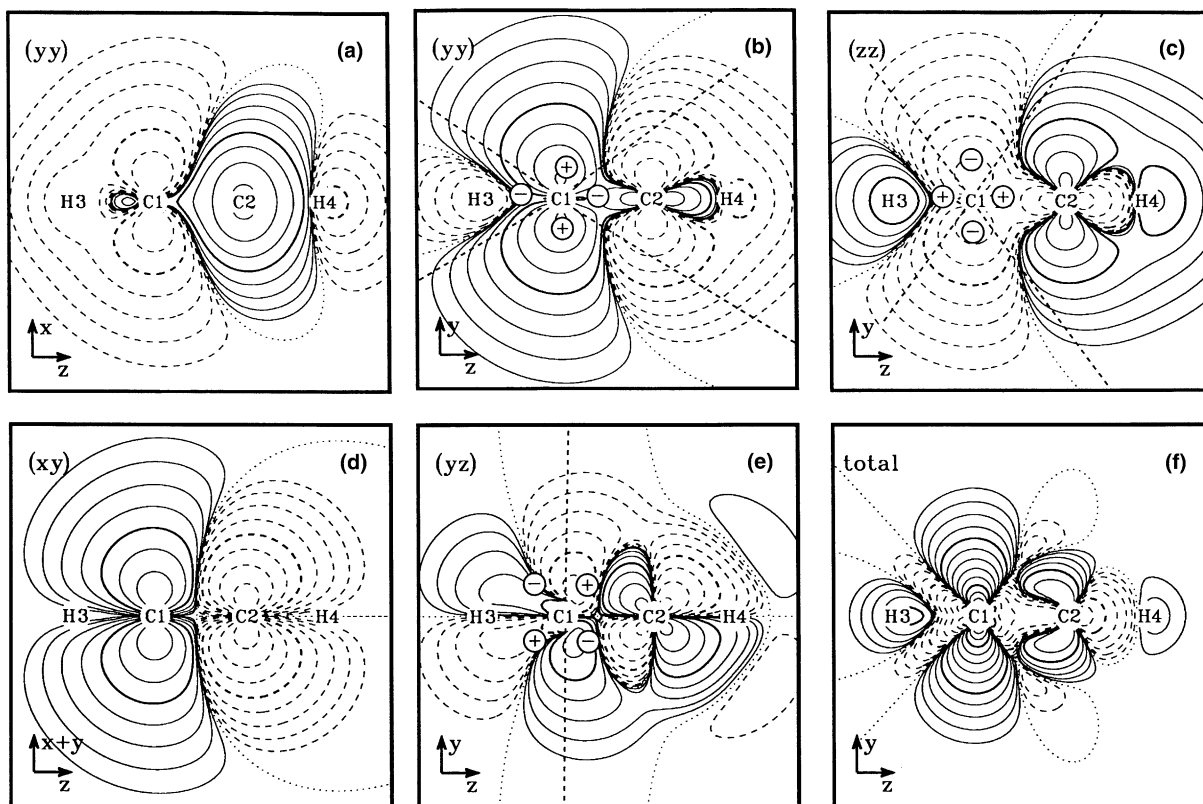
Fig. 2. Contour line diagrams of the SD spin polarization distribution and the SD energy density distribution of the SSCC ^1J(CC) for **1**. For each case the SD sub-component (ij) and the drawing plane is given. (a) SD spin polarization sub-component (yy) in the xz-plane, (b) SD spin polarization sub-component (yy) in the yz-plane, (c) SD spin polarization sub-component (zz) in the yz-plane, (d) SD spin polarization sub-component (xy) in the $x + y, z$-plane, (e) SD spin polarization sub-component yz in the yz-plane, and (f) total SD energy density distribution averaged over all orientations of the perturbing moment. - The perturbing nucleus is C2. All calculations done at the B3LYP/(11s,7p,2d/6s,2p)[7s,6p,2d/4s,2p] level of theory using the experimental geometry [30]. The contour levels are chosen equally tempered, i.e. in a geometric progression. The bold lines denote contour levels of 0.1 and 10; the relative spacing between two adjacent contours is $100^{1/5} = 2.5118864$. Solid lines denote positive, dashed lines negative, and the dotted lines a zero value of the SD spin polarization (or the SD energy density).

The contour line diagrams of $m_{B,(xx)}^{\mathrm{SD}}(\mathbf{r})$ (Fig. 2a; alternatively, this diagram can be viewed as the spin polarization distribution $m_{B,(yy)}^{\mathrm{SD}}(\mathbf{r})$) given in the xz-plane), $m_{B,(yy)}^{\mathrm{SD}}(\mathbf{r})$ (Fig. 2b), and $m_{B,(zz)}^{\mathrm{SD}}(\mathbf{r})$ (Fig. 2c) suggest a simple pattern for the SD spin polarization in the case of **1**. For the (yy) and (zz) diagram, the perturbing dipole moment at C2 is in the drawing plane oriented along the molecular axis ((zz) sub-component, Fig. 2c) or perpendicular to the molecular axis ((yy) sub-component, Fig. 2b). The SD spin polarization distribution reflects the shape of the dipole field in that it becomes negative (dominance of β-spin) along the direction of the dipole (where the field is parallel to the dipole moment; α-spin assumed for the C2 nucleus) and positive in the direction opposite to the dipole moment (where the dipole field is antiparallel to the dipole moment). In this way, the SD spin polarization distribution at C2 adopts the form of a $-d_{y^2}$ orbital in the case of the (yy) sub-component (Fig. 2b) and that of a $-d_{z^2}$ orbital in the case of the (zz) sub-component considering the signature of these two d-orbitals.

For the (xx) component, the perturbing dipole is perpendicular to the drawing plane. Since the (xx)- and (yy) sub-component of the SD term of ^1J(CC) of **1** are identical, Fig. 1a provides also a diagram of $m_{B,(yy)}^{\mathrm{SD}}(\mathbf{r})$ taken in the xz-plane. At C2, the SD spin polarization distribution is positive both in the yz-plane for $m_{B,(xx)}^{\mathrm{SD}}(\mathbf{r})$ or in the xz-plane for $m_{B,(yy)}^{\mathrm{SD}}(\mathbf{r})$. There are nodal planes leading to a sign inversion of the SD spin polarization distribution in the direction of H4 (Figs. 2a and b) and in the direction of C1. The former results from $\sigma \rightarrow \sigma^*$, the latter from the $\pi \rightarrow \pi^*$ excitations.

Generally, the different sub-components of the SD spin polarization distribution for a given molecule resemble each other. This can be rationalized by working out selection rules for the operators $h_{B,(ij)}^{\mathrm{SD}}$ dominating the actual operators $F_{B,(ij)}^{\mathrm{SD}}$ (see Eq. (12)). The operator $h_{B,(ij)}^{\mathrm{SD}}$ has the symmetry character of Cartesian d-functions at the perturbing nucleus B and accordingly has non-vanishing matrix elements for transitions of the kind s ↔ d, p ↔ f, d ↔ g,... and p ↔ p, d ↔ d, f → f,... where the s, p, d, f,... character of the orbitals

is considered with respect to nucleus B. In organic molecules, occupied as well as low-lying virtual d, f,... orbitals are not available, hence only $p \rightarrow p^*$ transitions can make sizable contributions to the SD term. Here and in the following, we use a shorthand notation to differentiate between MOs with p-character at B (p-MOs) from MOs with s-character at B (s-MOs). Hence, the excitation $p \rightarrow p^*$ denotes an excitation from an occupied MO with p-character to a virtual MO with p-character at B.

In detail, the following $p \rightarrow p^*$ transitions result in non-vanishing matrix elements for the individual components of the SD term:

$$h_{B,(xx)}^{SD} : p_x \rightarrow p_x^*, p_y \rightarrow -p_y^*, p_z \rightarrow -p_z^*, \tag{20a}$$

$$h_{B,(yy)}^{SD} : p_x \rightarrow -p_x^*, p_y \rightarrow p_y^*, p_z \rightarrow -p_z^*, \tag{20b}$$

$$h_{B,(zz)}^{SD} : p_x \rightarrow -p_x^*, p_y \rightarrow -p_y^*, p_z \rightarrow p_z^*, \tag{20c}$$

$$h_{B,(xy)}^{SD} : p_x \rightarrow p_x^*, p_y \rightarrow p_x^*, \tag{20d}$$

$$h_{B,(xz)}^{SD} : p_x \rightarrow p_z^*, p_z \rightarrow p_x^*, \tag{20e}$$

$$h_{B,(yz)}^{SD} : p_y \rightarrow p_z^*, p_z \rightarrow p_y^*. \tag{20f}$$

Here a negative sign in front of the virtual orbital means that the corresponding matrix element becomes negative, e.g., $p_x \rightarrow p_x^*$ for the (yy) sub-component means that $\langle p_x | h_{B,(yy)}^{SD} | p_x \rangle$ becomes negative. For the derivation of these selection rules, see Appendix A. One finds that all diagonal terms $h_{B,(ii)}^{SD}$ drive excitations from any occupied p orbital into any virtual p orbital of the same type. This explains why the different diagonal components of the SD spin polarization distribution possess similar patterns although their values can be quite different. A detailed analysis reveals (see Appendix A) that the excitations driven by $h_{B,(ii)}^{SD}$ lead to matrix elements larger in magnitude for a p_i than for a p_j $(j \neq i)$ function. The off-diagonal components $h_{B,(ij)}^{SD}$ $(j \neq i)$ drive excitations from p_i into p_j functions and vice versa.

The selection rules allow to rationalize the appearance of the SD spin polarization distribution as well as the trends in the orbital contributions to the SD terms of $^1J(CC)$ for **1–3**. In **1**, excitations from π orbitals into their π^* counterparts play the dominant role for the shape of the SD spin polarization distribution as well as for the value of the SD term. The diagonal terms $h_{A,(ii)}^{SD}$ drive excitations $\pi_x \rightarrow \pi_x^*$, $\pi \rightarrow \pi_y^*$. The degenerate π^* orbitals are C1–C2 antibonding, which explains the nodal plane in the SD spin polarization distribution between C1 and C2 in Figs. 2a–c.

Excitations from a σ- to a σ^*-orbital contribute to the SD spin polarization distribution provided the orbitals in question possess distinct p_σ character at C2. Considering the occupied all-bonding $2\sigma_g$, the CH-bonding

$2\sigma_u$, and the CC-bonding $3\sigma_g$ orbitals, only the latter has strong p_σ-character at the C atoms. Among the virtual orbitals $3\sigma_u$, $4\sigma_g$, and $4\sigma_u$, the first and the third possess more s- and the second more p_σ-character. Hence, the $3\sigma_g \rightarrow 4\sigma_g$ excitation contributes significantly to the diagonal SD spin polarization distribution components, which can be confirmed by the fact that these excitations must introduce nodal surfaces between the C and H atoms of **1** (see Figs. 2a–c).

The selection rules predict that the xy-cross term does not possess any p_z contribution (Eq. (20d)) and accordingly the nodal surfaces between C and H atoms are missing (see Fig. 2d; reference plane is the $x + y, z$ plane, which bisects the xz- and yz-planes; both the xz- and the yz-planes are nodal planes for this component). In this way, the (xy) component of the SD spin polarization distribution obtains a simple structure. There is a region with positive spin polarization around C1 and a region with negative spin polarization around C2 enveloping the dipole moment at C2 pointing into the positive $x + y$ direction; there are no further nodal planes in the density. The (yz) sub-component of the SD spin polarization distribution (Fig. 2e) is dominated by a spin polarization in the vicinity of nucleus C2 that has the shape of a d_{yz} function. The (xz) sub-component (not shown) is equivalent to the (yz) sub-component.

The total SD energy density distribution of **1**, shown in Fig. 2f in the yz-plane, is dominated by a torus with large positive values around C1 pointing into the xy-direction so that in Fig. 2f just a cut through this torus can be seen. There are smaller and less distinct positive regions in tori or spheres around C2, H3, and H4. In the three bond regions, the SD energy density is negative. Generally, the SD energy density is found by weighting each component of the SD spin polarization distribution $m_{B,(ii)}^{SD}(\mathbf{r})$ with the quadrupolar potential $h_{A,(ii)}^{SD}$ centered at the responding nucleus and being of the same type as that at the perturbing nucleus (see Eq. (14)). The isotropic SD term is then obtained by (a) calculating the total isotropic SD energy density $\varrho_{AB}^{SD}(\mathbf{r})$ (averaging over all ii-components), and (b) by integrating the isotropic SD energy distribution over all space.

The total SD energy density consists of many contributions with different character. However, many of these contributions can be rationalized by a simple rule: If the SD spin polarization distribution at the responding nucleus has partial d-character with the opposite (equal) signature as the spin polarization distribution at the perturbing nucleus, then the region around the responding nucleus will make a positive (negative) contribution to the SD energy density.

This can be seen most clearly for the (xy) term (Fig. 2d): the SD spin polarization distribution has d_{xy}-character both at the responding and the perturbing

nucleus, which can be seen when viewing $m^{SD}_{B,(xy)}(\mathbf{r})$ in planes through C1 and C2 perpendicular to the drawing plane of Fig. 2d. Due to the nodal surface of the SD spin polarization distribution between C1 and C2, these d_{xy} terms have opposite signs at C1 and C2, and the SD spin polarization distribution at C1 makes a large positive contribution to the SD energy density, which accounts for the large positive value (8 Hz, Table 2) of sub-component (xy). For the (yz) term (Fig. 2e), the SD spin polarization distribution has $-d_{yz}$-character both at the responding and the perturbing nucleus. Accordingly, the (yz) (and also the equivalent (xz)) term becomes negative (−1.4 Hz, Table 2). In y and z direction (Figs. 2b and c), the SD spin polarization distribution around C1 and C2 resembles d_{y^2} or d_{z^2} functions, which can be seen if one plots the SD spin polarization distribution $m^{SD}_{B,(yy)}(\mathbf{r})$ (i = y or z) in perpendicular planes as done in Fig. 2a in the case of i = y. Again, the functions around C1 and C2 have opposite signature and lead to positive contributions to the SD energy density and eventually large positive SD components (9.4 Hz each, Table 2).

The (yy) sub-component of the SD energy density (not shown) resembles actually the total SD energy

density: there is a cone with negative SD energy density oriented along the negative z-axis starting at C1 in the direction of H3 and a region with negative SD energy density around the C1C2 bond continuing towards H4. This pattern of the SD energy density can be derived when inspecting $m^{SD}_{B,(yy)}(\mathbf{r})$ in connection with the quadrupolar potential of Eq. (14). In Fig. 2b, dashed lines indicating the nodal surfaces of the quadrupolar potential generated by the perturbation $h^{SD}_{A,(ij)}$ are superimposed to the contour line diagram of $m^{SD}_{B,(yy)}(\mathbf{r})$. Also shown are the signs of this potential according to normal conventions. Multiplication of $m^{SD}_{B,(yy)}(\mathbf{r})$ with these signs leads directly to a SD energy density pattern similar to that of Fig. 2f. Similar considerations apply in the case of the (zz) sub-component of the SD energy density (compare Figs. 2c and f).

Since the SD energy density is preferentially positive as indicated in Figures such as 2f, all diagonal components (ii) of the SD term in 1 (9.42, 9.42, 5.43 Hz; Table 2) are positive, which also holds for the (ii) contributions form the individual π (C1C2) orbitals (Table 3), despite the fact the SD spin polarization distribution in the vicinity of the responding nucleus C1 has different signs

Table 3
Orbital contributions to the isotropic SD term and its sub-components (ij) calculated for ^1J(CC) of acetylene (**1**), ethylene (**2**), and ethane (**3**)[a]

Mol.	Orbital		Isotropic	(xx)	(yy)	(zz)	(xy)	(xz)	(yz)
1	C1–C2	σ	−1.231	−1.231	−1.231	−0.566	0.018	−0.729	−0.729
2	C1–C2	σ	−0.738	−0.013	0.196	0.328	−0.012	0.143	−1.494
3	C1–C2	σ	0.783	0.357	0.357	1.457	−0.007	0.049	0.049
1	C1–C2	π_x	6.707	8.331	1.165	3.110	3.964	−0.207	−0.000
1	C1–C2	π_y	6.707	1.165	8.331	3.110	3.964	−0.000	−0.207
2	C1–C2	π	5.096	2.368	11.384	3.351	0.027	0.003	0.938

[a] All values in Hz as calculated at the CP-DFT/B3LYP/(11s,7p,2d/6s,2p)[7s,6p,2d/4s,2p] level of theory using experimental geometries [30–32]. See also footnote in Table 2.
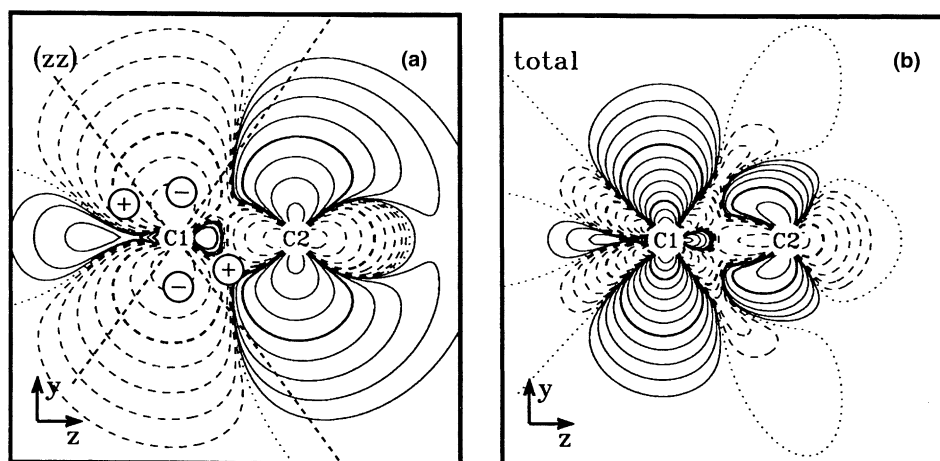

Fig. 3. Contour line diagrams of the SD spin polarization and SD energy density distribution of the SSCC ^1J(CC) for **2**. (a) SD spin polarization distribution sub-component (zz), (b) total SD energy density averaged over all orientations of the perturbing moment. The perturbing nucleus is C2. All calculations done at the B3LYP/(11s,7p,2d/6s,2p)[7s,6p,2d/4s,2p] level of theory using the experimental geometry [31]. See also Fig. 2.

for (yy) than for (xx) or (zz). Table 3 reveals that for a π_y orbital, the (yy) sub-component of the orbital SD contribution is larger than the (xx) and (zz) sub-components. This is in line with selection rule (20b), which indicates that $h_{B,(yy)}^{SD}$, drives excitations from p_y orbitals more efficiently (leading to larger magnitudes of the corresponding matrix elements) than either $h_{B,(xx)}^{SD}$ (rule (20a)) or $h_{B,(zz)}^{SD}$ (rule (20c)) does. Analogously, this applies also to the weighting of the SD spin polarization distribution at C1, which explains that the (xx) and (yy) components of the π_y(C1C2) orbital contributions differ by a factor of 7.2 for **1** (1.17 and 8.33 Hz, Table 3).

Fig. 3a gives the (zz) sub-component of the SD spin polarization for **2**. The SD spin density resembles markedly the (zz) SD spin polarization distribution of **1**. Analogously, the (xx) and (yy) sub-components, which are not shown in Fig. 3, resemble their counterparts for **1**. The total SD energy density (Fig. 3b), which in turn is similar to that of **1**, is strongly dominated by its (yy) term, which is also reflected in the

large (yy) component of the SD term (11.3 Hz, Table 2). The dominance of the (yy) term is due to the effect of the $p_y \rightarrow p_y^*$ excitation, i.e. the only possible excitation in the π system of **2**. It is noteworthy that the (yy) sub-component of the π_y(C1C2) orbital contribution is larger for **2** than for **1** because of the well-known fact that the $\pi_y \rightarrow \pi_y^*$ excitation energy is smaller for **2** than for **1** (calculated B3LYP/[7s,6p,2d/4s,2p] orbital energies for 1 are: −0.30085 (π) and 0.01338 (π^*); excitation energy: 0.31423 hartree; and for **2**: −0.27991 (π) and −0.01170 (π^*); excitation energy: 0.26821 hartree). In **2**, excitations from the π_y into the pseudo-π_x^* orbital requires a relatively large energy and therefore the corresponding (xy) sub-component in **2** is small (0.03 Hz, Table 3).

The diagonal SD spin polarization sub-components for **3**, which are shown in Figs. 4a–c, agree with the SD spin polarization distributions of **1** and **2** in a number of ways: The diagonal sub-components of the SD spin polarization are dominated by two large regions around
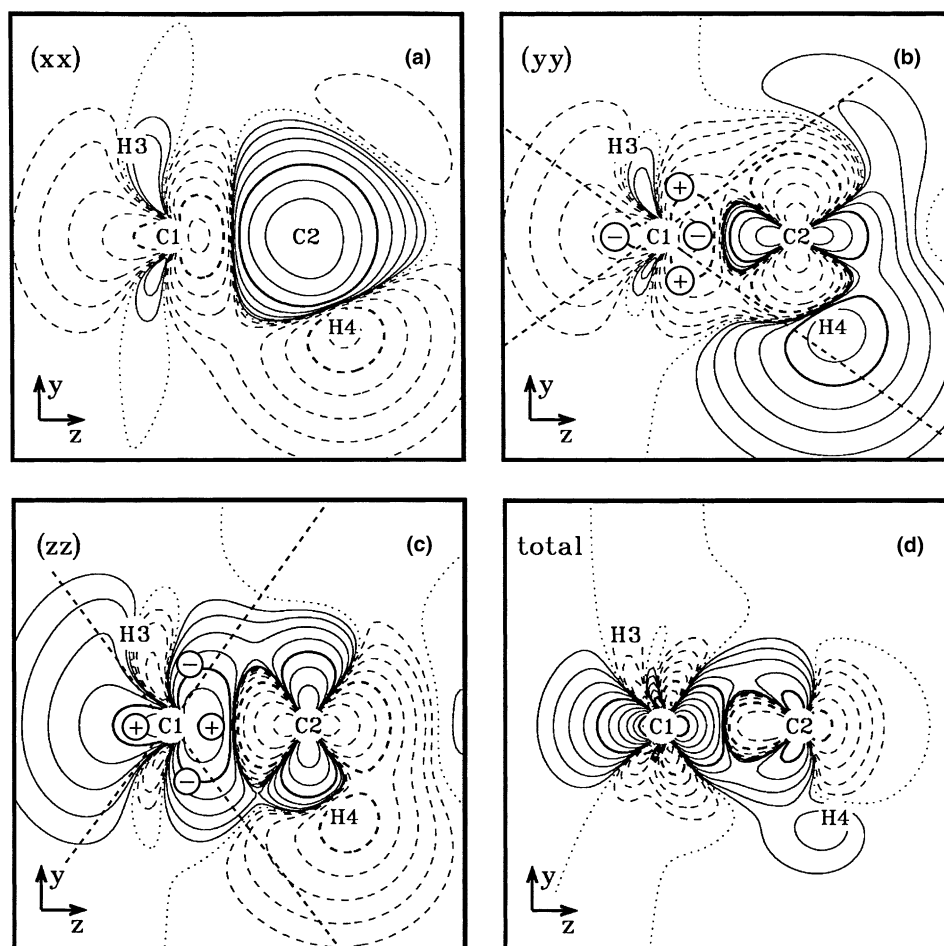

Fig. 4. Contour line diagrams of the SD spin polarization and SD energy density distribution of the SSCC ^1J(CC) for **2**. (a) SD spin polarization sub-component (xx), (b) SD spin polarization sub-component (yy), (c) SD spin polarization sub-component (zz), and (d) total SD energy density distribution averaged over all orientations of the perturbing moment. The perturbing nucleus is C2. All calculations done at the B3LYP/(11s,7p,2d/6s,2p)[7s,6p,2d/4s,2p] level of theory using the experimental geometry [32]. See also Fig. 2.

C1 and C2 with negative or positive SD spin density and a nodal plane in between. Whereas for the (xx) and (yy) sub-component, the region around C1 has preferentially negative spin polarization, it has positive spin polarization for the (zz) sub-component. The SD spin polarization around C2 reflects the shape of the dipole field in the same way as described above for **1**. Special for **3** is that the spin polarization is more concentrated around the C1-C2 axis than for either **1** or **2**. Also, there is an extended region around H4 that has a spin polarization opposite to that around C2. Again the sign-pattern of the total SD energy density is easily derived from Figs. 4b and c by combining the sign of $m_{B,(ii)}^{SD}(\mathbf{r})$ ($i = y$ or z) with that of the quadrupolar potential as indicated in the contour line diagrams. The total SD energy density is dominated by a region with positive values close to C1 around the C1C2 bond axis. All three diagonal sub-components contribute to this region, the largest contribution coming from the (zz) sub-component.

Table 3 lists the dominant orbital contributions to $^{1}SD(CC)_{(ij)}$ in Hz. The SD term is largely determined by contributions from the occupied π-orbitals whereas some smaller contributions arise from the CC σ-bond orbital. The total SD contribution per π orbital in **1** is larger than for the π-orbital in **2** (6.7 vs 5.1 Hz, Table 3). This can be traced back to the large positive (xy) SD contribution in **1** (4.0 Hz as compared to 0.03 Hz in **2**). For the σ(C1C2) bond orbital, the isotropic SD contribution becomes more negative with increasing number of π bonds between C1 and C2: the contribution of this orbital to the SD term is 0.78 Hz for **3**, −0.74 Hz for **2**, and −1.23 Hz for **1** (Table 3). This trend can be traced back to the behavior of the (zz) component, which decreases from 1.46 (**3**) to −0.57 Hz (**1**).

The σ(C1C2) orbital SD contributions are dominated by the equivalent (xz) and (yz) components in **1** and the (yz) sub-component in **2**. The operator $h_{A,(yz)}^{SD}$ drives excitations from the σ(C1C2) orbital, which has

partial p_{σ} character at C2, into the virtual π_{y}^{*} orbital. The absolute value of the component is larger for **2** than for **1**, which is due to the stronger p-character of the σ(C1C2) orbital (sp^{2} rather than sp). For all three molecules, the (zz) components make a significant contribution to the SD term. This contribution becomes more positive in the order **1**, **2**, **3**. This can be understood from the (zz) SD spin polarization diagram of this orbital contribution (see Fig. 5). Whereas for **1**, the SD spin polarization density is uniformly negative in the region of the σ(C1C2) bond surrounded by a ring of uniformly positive SD spin density (Fig. 5a), it possesses a nodal plane between C1 and C2 for **2** (Fig. 5b) and for **3** (Fig. 5c).

The (zz) sub-component of the σ(C1C2)-orbital SD contribution is related to excitations into σ^{*} orbitals. There one has to consider those σ- and σ^{*}-orbitals, which possess distinct p_{σ}-character but little s-character both at the perturbing and responding nucleus. These are the CC-bonding $3\sigma_{g}$-orbital and the CH-antibonding $4\sigma_{g}$-orbital (rather than the lower lying CC-antibonding $3\sigma_{u}$-orbital) in the case of **1**, the CC-bonding $3a_{g}$-orbital and CC-, CH$_2$-antibonding $3b_{1u}$-orbital (rather than the CH$_2$-antibonding $4a_{g}$-orbital) in the case of **2** as well as the CC-bonding $3a_{1g}$-orbital and CC-antibonding $3a_{2u}$-orbital in the case of **3**. The three occupied orbitals are all CC bonding, which implies that they decrease in energy from **3** to **1** because of the shortening of the CC bond. In the same direction, the virtual orbitals increase in energy thus leading to increasing $\sigma \rightarrow \sigma^{*}$ excitation energies from **3** to **2** and **1**, which behave like 1.1:1.15:1.3 (B3LYP/[7s,6p,2d/4s,2p] calculations). The corresponding SD spin polarization distribution must be largest for **3** and smallest for **1** (Fig. 5) and the corresponding (zz) sub-components of the σ(CC) orbital must decrease in the same direction (1.46, 0.33, −0.57 Hz; Table 3). Since the $4\sigma_{g}$-orbital of **1** does not possess a nodal plane cutting through the C1C2 bond, there is no sign in-
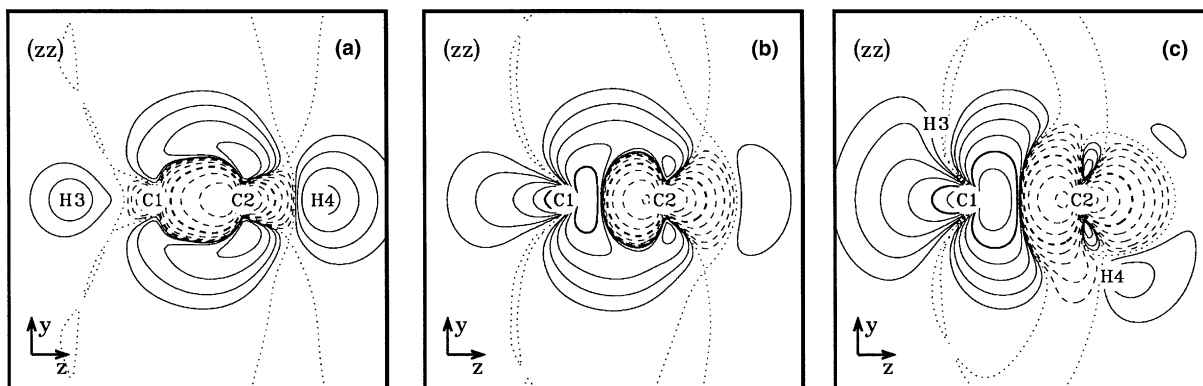

Fig. 5. Contour line diagrams of the SD spin polarization distribution of sub-component (zz) caused by orbital σ(C1C2). (a) **1**, (b) **2**, (c) **3**. The perturbing nucleus is C2. All calculations done at the B3LYP/(11s,7p,2d/6s,2p)[7s,6p,2d/4s,2p] level of theory using the experimental geometries [30–32]. See also Fig. 2.

version of the SD spin polarization distribution along the CC axis for this molecule (Fig. 5a).

4. Chemical relevance of results and conclusions

Despite the fact that three diagonal ii-components equivalent to six (ij) sub-components (see Eq. (15)) contribute to the isotropic SD term, each of which can be decomposed into σ- and π-contributions, and despite the fact that the isotropic SD term has to be analyzed stepwise by considering first the SD spin polarization distribution, then the SD energy density distribution, integrating over the total space for each sub-component of the SD energy density, and finally averaging over all directions, the behavior of the total SD term can be simply described as being governed by two opposing trends: (i) The contributions from the π bond orbitals become more positive the more π bonds are present, (ii) The contribution from the $\sigma(C1C2)$ bond orbital becomes more negative with increasing π-character of the bond. Trend (i) is stronger and thus determines the behavior of the total SSCC.

Trends (i) and (ii) provide a basis to relate the magnitude of the SD term of SSCC $^1J(CC)$ to the π-character of a bond. Clearly, there is no experimental way to separate the SD part of $^1J(CC)$ from the FC and the other non-contact (NC) terms. There is the possibility of estimating the sum of the NC terms of SSCC $^1J(CC)$ utilizing measured $^1J(CC)$ values and the SSCCs $^1J(CH)$ or $^1J(CC)$ from all adjoined bonds [22]. It was shown that there is a cubic dependence of the NC terms of $^1J(CC)$ on the π bond order, which is dominated by the PSO term [22]: For CC double bonds, the PSO term adopts large negative values, for CC single bonds values close to zero, and for triple bonds large positive values. It is difficult to see, without extra-calculations, whether the NC term of $^1J(CC)$ in a conjugated CC bond such as in benzene or for the CC double bond in a cumulene is positioned on the decreasing or increasing branch of the cubic function.

The SD term is easier to read because it depends in an exponential rather than cubic way on the π-character of a CC bond (Fig. 1), which can be traced back to trends (i) and (ii). Clearly, the SD term, of $^1J(CC)$ represents a magnetic antenna that can be used as quantum chemical descriptor for bonding. In this work we have set the basis for analyzing the SD part of SSCCs.

(1) The SD spin polarization distribution $m^{SD}_{B,(ij)}(\mathbf{r})$ defined in this work (Eq. (16a)) helps to visualize the first step of the SD spin–spin coupling mechanism, i.e. the spin polarization of the electron system by the perturbing nucleus.

(2) At the perturbing nucleus, the SD spin polarization is determined by the dipole field of the nuclear spin moment. Along the axis of the latter, spin polarization is dominated by β-, perpendicular to it by α-spin assuming α-spin for the nuclear moment.

(3) The SD spin polarization distribution at the responding nucleus depends on the excitations from occupied to virtual spin orbitals involved in the definition of $m^{SD}_{B,(ij)}(\mathbf{r})$ according to Eqs. (16a) and (11). For these excitations the following applies:

(4) The orbitals contributing to the SD spin polarization distribution must possess distinct p-character (p_σ or p_π) and low s-character at both the perturbing and responding nucleus. This is true for all π orbitals but only for a subset of the σ orbitals as discussed for molecules **1**, **2**, and **3**.

(5) The selection rules worked out in this investigation and listed in Eqs. (20) provide the sign of the corresponding matrix element defined in Eq. (13). They also make it possible to predict relative values.

(6) The magnitude of the matrix element (13) is strongly determined by the energy gap between occupied and virtual orbitals, which influences also the magnitude of the SD sub-components.

(7) The SD energy density defined in this work (see Eq. (16b)) is obtained by weighting the SD spin polarization distribution with the quadrupolar potential of the operator $h^{SD}_{A,(ij)}$. The signature of the SD energy density is easily obtained by determining the local character of the SD spin polarization (ij) at responding nucleus A and combining it with the signature of the quadrupole potential $h^{SD}_{A,(ij)}$ (see Figs. 2–4).

(8) There is a simple relationship between the SD spin polarization distribution and the SD energy density distribution: If the former has partial d-character at the responding nucleus with the opposite (equal) signature as the spin polarization distribution at the perturbing nucleus, then the region around the responding nucleus will make a positive (negative) contribution to the SD energy density.

(9) For acetylene, ethylene, and ethane, all diagonal sub-components $J^{SD}_{AB,(ii)}$ are positive, however most important is the (xx) sub-component, which determines the exponential increase of the isotropic SD term with the bond order.

Work is in progress to apply rules (1)–(8) for analyzing the SD term in molecules with hetero atoms.

computer time. JG thanks Carl Tryggers Stiftelse for financial support.

Appendix A

In this appendix, the selection rules for operators $h^{SD}_{B,(ij)}$ used in Section 3 are derived. For that purpose, we write down the results for the multiplication of selected real p and d functions where the latter represent the quadrupole potential of $h^{SD}_{B,(ij)}$. These results can be found either from the corresponding Clebsch–Gordan coefficients or by inspection from the explicit expressions of the spherical functions. It holds

$$p_z d_{z^2} = \frac{1}{4\pi}\left[\sqrt{\frac{4}{5}}p_z + \sqrt{\frac{27}{35}}f_{z^3}\right], \tag{A.1a}$$

$$p_z d_{x^2} = \frac{1}{4\pi}\left[-\sqrt{\frac{1}{5}}p_z + \sqrt{\frac{18}{35}}f_{x^2z}\right], \tag{A.1b}$$

$$p_z d_{xz} = \frac{1}{4\pi}\left[p_z + \sqrt{\frac{8}{35}}f_{xz^2}\right], \tag{A.1c}$$

$$p_z d_{xy} = \frac{1}{4\pi}\sqrt{\frac{1}{7}}f_{xyz}. \tag{A.1d}$$

Here we have used the definitions

$$p_z = \sqrt{\frac{3}{4\pi}}\hat{z}, \tag{A.2a}$$

$$d_{z^2} = \sqrt{\frac{15}{4\pi}}(3\hat{z}^2 - 1), \tag{A.2b}$$

$$d_{x^2} = \sqrt{\frac{15}{4\pi}}(3\hat{x}^2 - 1), \tag{A.2c}$$

$$d_{xz} = \sqrt{\frac{5}{4\pi}}\hat{x}\hat{z}, \tag{A.2d}$$

$$d_{xy} = \sqrt{\frac{5}{4\pi}}\hat{x}\hat{y}, \tag{A.2e}$$

$$f_{z^3} = \sqrt{\frac{7}{16\pi}}(5\hat{z}^3 - 3\hat{z}), \tag{A.2f}$$

$$f_{x^2z} = \sqrt{\frac{21}{32\pi}}(5\hat{x}^2 - 1)\hat{z}, \tag{A.2g}$$

$$f_{xz^2} = \sqrt{\frac{21}{32\pi}}\hat{x}(5\hat{z}^2 - 1), \tag{A.2h}$$

$$f_{xyz} = \sqrt{\frac{105}{4\pi}}\hat{x}\hat{y}\hat{z}, \tag{A.2i}$$

where $x = x/r$, etc. Note that we, in distinction to common usage in atomic theory, have to consider spherical functions referring to different quantization axes (x, y, and z). This implies that not all of the spherical functions occurring in Eqs. (A.1a)–(A.1d) and (A.2a)–(A.2i) are orthogonal to each other: d_{z^2} is not orthogonal to d_{x^2}, f_{x^2z} not to f_{xz^2}. Of course, spherical harmonics belonging to different values of the angular momentum are always orthogonal to each other.

Multiplication of (A.1a) from the right with p_z leads to a positive non-vanishing term (see rule 20c). Cyclic exchange of the indices leads to the remaining selection rules given in Section 3.

References

[1] See, e.g.D.M. Grant, R.K. Harris (Eds.), Encyclopedia of Nuclear Magnetic Resonance, vols. 1–8, Wiley, Chichester, 1996.
[2] J.A. Pople, W.G. Schneider, H.J. Bernstein, High-resolution Nuclear Magnetic Resonance, McGraw-Hill, New York, 1959.
[3] J.W. Emsley, J. Feeney, L.H. Sutcliffe, High Resolution Nuclear Magnetic Resonance Spectroscopy, Pergamon, Oxford, 1966.
[4] V.I. Minkin, M.N. Glukhovtsev, B.Y. Simkin, Aromaticity and Antiaromaticity, Electronic and Structural Aspects, Wiley, New York, 1994.
[5] B.Y. Simkin, V.I. Minkin, M.N. Glukhovtsev, in: A.R. Katritzky (Ed.), Advances in Heterocyclic Chemistry, vol. 56, Academic Press, San Diego, 1993, p. 303.
[6] A.R. Katritzky, K. Jug, D.C. Oniciu, Chem. Rev. 101 (2001) 1421.
[7] P.v.R. Schleyer, P.K. Freeman, J. Giao, B. Goldfuss, Angew. Chem. Int. Ed. Engl. 34 (1995) 337.
[8] P.v.R. Schleyer, C. Maerker, D. Dransfield, H. Jioa, J.R. van Eikema Hommes, J. Am. Chem. Soc. 118 (1996) 6317.
[9] N. Muller, D.E. Pritchard, J. Chem. Phys. 31 (1959) 768.
[10] M.D. Newton, J.M. Schulman, M.M. Manus, J. Am. Chem. Soc. 96 (1974) 17.
[11] R.M. Lynden-Bell, N. Sheppard, Proc. Roy. Soc. A 269 (1962) 385.
[12] K. Frei, H.J. Bernstein, J. Chem. Phys. 38 (1963) 1216.
[13] J. Wardeiner, W. Lüttke, R. Bergholz, R. Machinek, Angew. Chem. Int. Ed. Engl. 21 (1982) 872.
[14] K. Kamienska-Trela, Spectrochim. Acta A 36 (1980) 239.
[15] H. Günther, NMR-Spectroscopy, Thieme, New York, 1983.
[16] H.O. Kalinowski, S. Berger, S. Braun, ¹³C-NMR-Spektroskopie, Georg Thieme Verlag, Stuttgart, 1984.
[17] N.F. Ramsey, Phys. Rev. 91 (1953) 303.
[18] V. Sychrovský, J. Gräfenstein, D. Cremer, J. Chem. Phys. 113 (2000) 3530.
[19] A. Wu, J. Gräfenstein, D. Cremer, J. Phys. Chem. 107 (2003) 7043.
[20] J. Gräfenstein, T. Tuttle, D. Cremer, J. Am. Chem. Soc. (submitted).
[21] J. Gräfenstein, D. Cremer, Chem. Phys. Lett. 383 (2004) 332.
[22] D. Cremer, E. Kraka, A. Wu, W. Lüttke, Chem. Phys. Chem. (in press).
[23] J. Gräfenstein, D. Cremer, J. Phys. Chem. A (submitted).
[24] T. Tuttle, A. Wu, E. Kraka, D. Cremer, J. Am. Chem. Soc. (in press).
[25] T. Tuttle, J. Gräfenstein, A. Wu, E. Kraka, D. Cremer, J. Phys. Chem. B 108 (2004) 115.
[26] A.D. Becke, Phys. Rev. A 38 (1988) 3098.
[27] C. Lee, W. Yang, R.P. Parr, Phys. Rev. B 37 (1988) 785.
[28] A.D. Becke, J. Chem. Phys. 98 (1993) 5648.

[29] W. Kutzelnigg, U. Fleischer, M. Schindler, in: NMR – Basic Principles and Progress, vol. 23, Springer, Heidelberg, 1990, p. 165.

[30] A. Baldacci, S. Ghersetti, S.C. Hurlock, K.N. Rao, J. Mol. Spectrosc. 39 (1976) 116.

[31] H.C. Allena, E.K. Plyler, J. Am. Chem. Soc. 80 (1958) 2673.

[32] E. Hirota, K. Matsumara, M. Imachi, M. Fujio, Y. Tsuno, J. Chem. Phys. 66 (1977) 2660.

[33] E. Kraka et al., COLOGNE 2003, Göteborg University, Göteborg, 2003.